

DRAFT\* DRAFT \* DRAFT \*

November7, 1997, 3:26pm

\* DRAFT \* DRAFT \* DRAFT

**Optimal Detection of Global Warming using Temperature Profiles**

STEPHEN s. LEROY

*Jet Propulsion Laboratory, California Institute of Technology, Pasadena, California*

Manuscript Submitted November ??, 1997

*Corresponding author address: Dr. Stephen Leroy, Earth and Space Sciences Division,  
Jet Propulsion Laboratory, mail stop 183-335, Pasadena, CA 91109*

## ABSTRACT

Optimal fingerprinting is applied to estimate the amount of time it would take to detect warming by increased concentrations of carbon dioxide in monthly averages of temperature profiles over the Indian Ocean. A simple radiative-convective model is used to define the structure of the warming signal, and the 100-year control run of the GFDL atmospheric oceanic global climate model is used to estimate the natural variability of the upper air temperatures. The signal is assumed to be the difference in two periods of data, each period consisting of twelve consecutive months of monthly average temperature profiles. When the variability of monthly averages are assumed independent of each other, the difference in August upper-air temperatures yielded the strongest fingerprint, giving a time span for a 1-sigma detection of **22** years. When only August surface temperatures are used, the 1-sigma detection time is **43** years. When correlations of natural variability between months are considered, the 1-sigma detection time becomes 10 years, 13 years for surface temperatures.

In optimal fingerprinting the detection times can be critically dependent on small, uncertain aspects of the signal shape used to detect a particular signal. The methods used to eliminate such a possibility are *ad hoc* in this work, yet a formal method to properly handle such difficulties should be constructed in the future.

## 1. Introduction

That the near-surface temperature of the Earth's atmosphere has been increasing over the last several decades is almost certain; however, whether the warming is attributable to increasing levels of greenhouse gas concentrations is still questionable (IPCC 95). The issue of attributability is commonly addressed by looking for distinctive features in the pattern of the observed warming which are predicted by theoretical models of the climate system. Recent pattern-based studies have examined surface temperature data from the past century (Hegerl et al. 1996, 1997) and radiosonde records from the past 50 years (Santer et al. 1995, 1996). Only the former used a formal statistical technique known as "optimal fingerprinting," which specifically weights those components of the expected pattern so that much of the natural variability of the climate is eliminated (Bell 1986, Hasselmann 1993, North et al. 1995). The result is a signal-to-noise ratio (or a time-series of signal-to-noise ratios), which gives the probability that a natural fluctuation of the climate could explain the trend that is seen in the climatological data.

Leroy (1998) has shown that the technique of optimal fingerprinting is a special case of Bayesian statistics in which the pattern of the signals are assumed as known and the unknowns are the amplitudes of the signals to be detected. Consequences of this approach are (1) that optimal fingerprinting is able to perfectly distinguish between different forced climate signals, no matter how similar their patterns, and (2) that any error in the prescription of the signal patterns leads to confusing the detection of one forced climate signal for another. The first allows us to detect several forced signals without having to impose *a priori* conditions on the ratios of the signal amplitudes to be detected, and the second dictates that care must be taken when relying upon signal patterns which are to be used in climate signal detection studies.

The results of the pattern-based signal detection studies to date, most of which concentrate on global-scale horizontal patterns (Hegerl et al. 1996, 1997), point toward a human influence on present trends in the Earth's climate (IPCC 95). This

conclusion, though, is largely based on the absence of substantial long-term natural variability of the climate as prescribed by long control runs of atmosphere/ocean global climate models (AOGCM's). Many AOGCM's contain a "flux adjustment" in order to maintain realistic climate states in cases where ocean circulation tends to magnify discrepancies in the surface energy balance (Manabe et al. 1995). This type of adjustment could suppress some interdecadal variability which the ocean circulation might realistically generate. If indeed there is increased interdecadal variability caused by changes in the ocean circulation, one need not rely on improved modeling to differentiate such variability from trends caused by increased greenhouse gas forcing. For instance, it is expected that a change in ocean circulation ought to impact the vertical structure of the atmosphere differently than does warming by increasing concentrations of greenhouse gases. Furthermore, the pattern of stratospheric cooling and tropospheric warming by increasing greenhouse gas concentrations may be quite different than natural climate patterns of tropospheric and stratospheric fluctuations. Thus, we are pointed toward the necessity of applying pattern-based studies to changes in the vertical structure of the climate.

The data sets available at present for pattern-based studies are unsuitable because they either suffer from calibration error or incomplete global coverage. For instance, the 50-year record of radiosonde measurements (Angell 1988) suffer from both inadequacies (Gaffen 1994). With the scheduled launching of instruments such as the Atmospheric Infrared Sounder (Aumann and Pagano 1994) as part of EOS, we can expect a deluge of data which is potentially suitable for pattern-based studies of changes in the vertical structure of the atmosphere. In addition, two remote sensing experiments have been proposed which would obtain global coverage with negligible calibration error: one of which is radio occultation of the atmosphere using the global positioning system (Kursinski et al. 1996, 1997, Leroy 1997) and the other is a high resolution infrared interferometer, both of which are low cost (Goody et al. 1997).

In this paper, optimal fingerprinting is used to investigate the likelihood of detecting changes in vertical temperature which are attributable to increasing concentrations of greenhouse gases. For the sake of simplicity, only temperature profiles in the region of the Indian Ocean are considered, and it is anticipated that the data set to be obtained is only one year in length. This snapshot of the atmosphere would then be compared to a similar snapshot of the atmosphere several years hence to identify trends possibly attributable to increasing greenhouse gas concentrations. Even though raw measurements can be used in optimal fingerprinting, such as infrared radiances from AIRS or an interferometer or refractivities from GPS radio occultations, in this study temperature profiles are used.

In the second section of this paper a brief introduction to optimal fingerprinting is presented following Hasselmann (1993, 1997). In the third section is an analysis of how long it should take to positively attribute a trend in the temperature profile to greenhouse-gas induced warming if it is indeed present. This analysis first assumes that only an individual month of data is taken in each of the two snapshots of the atmosphere over the Indian Ocean and then assumes that an entire year's worth of monthly averages is taken in each snapshot. The final section of this paper is a discussion of the implications of this work and work which must be done in the future.

## **2.0 Optimal fingerprinting**

In a pattern-based detection study, it is anticipated that we have  $N$  data elements which comprise a data vector  $d$ . The elements of this vector can be any type of measurement or post-processed measurement such as temperature as measured by a surface meteorological station, a temperature at 300 mbars as retrieved from a radiance measurement from space, a monthly mean geopotential height of the 200-mbar surface over a specific location, etc. Furthermore, it is required that a climatological mean is removed from  $d$ . This can be done in many ways. For instance, if an element is a Fourier transform component of a time series, no mean is involved. Also, one can take two

snapshots of the atmosphere and take the difference of like elements, thus eliminating a climatological mean. In the end, the data vector with  $N$  elements can be written as

$$\underline{d} = \sum_{i=1}^m \underline{S}_i \alpha_i + \underline{n} \quad (1)$$

in which  $m$  signals are hypothesized to be present, the  $i$ 'th signal is expected to have a pattern  $\underline{S}_i$  as seen in the data, the amplitude of the  $i$ 'th signal is  $\alpha_i$ , and  $\underline{n}$  is a Gaussian noise component which describes the natural variability of the atmosphere as seen in the data  $\underline{d}$ . Each of the  $m$  signals is the response in the data to an "external" forcing, such as variations in solar insolation due to the 11-year solar cycle, decreasing levels of stratospheric ozone, etc. The statistics of the climate variability component can be adequately described by its covariance

$$\mathbf{N} = \langle \underline{n} \underline{n}^T \rangle. \quad (2)$$

The signal patterns can be rewritten in the form of a matrix  $\mathbf{S}$  with  $N$  rows and  $m$  columns, the  $i$ 'th column of which is the pattern of the  $i$ 'th signal  $\underline{S}_i$ .

At first it is instructive to find signal amplitudes given signal patterns  $\mathbf{S}$  without regard to the nature of the climate variability. This is done by define  $\chi^2$  as

$$\chi_{\text{nonoptimal}}^2 = (\underline{d} - \mathbf{S}\alpha)^T (\underline{d} - \mathbf{S}\alpha) \quad (3)$$

which is simply the sum of the square of residuals after the signals are removed from the data. The signal amplitudes are found by minimizing  $\chi_{\text{nonoptimal}}^2$  by varying it in  $\alpha$ . The solution is

$$\alpha_{\text{nonoptimal}} = \mathbf{C}_{\text{nonoptimal}}^T \underline{d} \quad (4a)$$

where

$$\mathbf{C}_{\text{nonoptimal}} = \mathbf{S}(\mathbf{S}^T \mathbf{S})^{-1} \quad (41)$$

The columns of  $\mathbf{C}_{\text{nonoptimal}}$  make up a set of vectors called signal adjoints, the  $i$ 'th column of  $\mathbf{C}_{\text{nonoptimal}}$  projecting only onto the  $i$ 'th column of  $\mathbf{S}$  and no other. In this case, note that the adjoint vectors which comprise  $\mathbf{C}_{\text{nonoptimal}}$  span the same space as

the vectors which comprise  $\mathbf{S}$ . Using the adjoint vectors, it is possible to detect signals with the patterns prescribed by  $\mathbf{S}$  by simply cross-correlating them with the data set  $d$ . This pattern-based detection method is nonoptimal, though.

Detection can be optimized by redefining  $\chi^2$ , essentially dividing the residuals by the noise. In doing so, large residuals are permitted where the natural variability of the climate is expected to be large anyway, but residuals are more strongly penalized where the climate is not expected to vary naturally by very much. The redefinition is

$$\chi_{\text{optimal}}^2 \equiv (d - \mathbf{S}\alpha)^T \mathbf{N}^{-1} (d - \mathbf{S}\alpha). \quad (5)$$

The signal amplitude  $\alpha$  which minimizes  $\chi_{\text{optimal}}^2$  is found, as usual, by varying  $\alpha$  and setting  $\delta\chi_{\text{optimal}}^2 = 0$ . The result is the “most probable” signal amplitude  $\alpha_m$ , which is

$$\alpha_m = \mathbf{C}^T d \quad (6a)$$

where

$$\mathbf{C} = \mathbf{N}^{-1} \mathbf{S} (\mathbf{S}^T \mathbf{N}^{-1} \mathbf{S})^{-1}. \quad (6b)$$

The columns of  $\mathbf{C}$  are the optimal adjoints of the signal patterns given by the columns of  $\mathbf{S}$ . Once again, the  $i$ 'th optimal adjoint pattern has a nonzero correlation with only the  $i$ 'th signal pattern  $S_i$ . The space spanned by the optimal adjoints is that spanned by the eigenvectors of  $\mathbf{N}$ .

The uncertainty in the calculated amplitude  $\alpha_m$  is a covariance matrix  $\mathbf{A}$  in the elements of  $\alpha$ . The uncertainty in the amplitude of the  $i$ 'th signal is just the square root of the  $i$ 'th diagonal element of  $\mathbf{A}$ . This covariance matrix is found by varying the data  $d$  by the natural variability  $\eta$ , estimating the change in the signal amplitude  $\delta\alpha = \mathbf{C} \eta$ , and calculating the ensemble average

$$\mathbf{A} \equiv \langle \delta\alpha \delta\alpha^T \rangle \quad (7)$$

which yields

$$\mathbf{A} = (\mathbf{S}^T \mathbf{N}^{-1} \mathbf{S})^{-1}. \quad (8)$$

The uncertainty in the signal amplitudes can be determined given the prescription of the signal patterns and the natural variability but without, any real data.

While the theory is elegant and all the quantities are well-defined, working with the natural variability covariance matrix  $\mathbf{N}$  can be problematic. In general, one would compute the natural variability matrix by taking the ensemble average of climate fluctuations, as in Eq. (2), from a long control run of an AOGCM. The dimension of  $\mathbf{N}$  is the number of members in the data vector  $\underline{d}$ , which can be a large number indeed. If an ensemble of 100 elements is used to calculate  $\mathbf{N}$ , then if its rank  $\mathbf{N}$  is greater than 100, the matrix  $\mathbf{N}$  will have at least  $\mathbf{N} - 101$  eigenvalues which are zero. In that case,  $\mathbf{N}$  cannot be inverted. This problem is avoided if we retain only the first  $l$  eigenmodes of  $\mathbf{N}$  as suggested by Hasselman (1993). In this situation, the eigenvalues of  $\mathbf{N}$  are  $\lambda_k$  and the eigenvectors are  $\underline{P}_k$ ,  $\underline{P}_k$  being the  $k$ 'th column of matrix  $\mathbf{P}$ . If only a subset of 1 eigenmodes is retained, then a truncated noise covariance matrix and its inverse are defined as

$$\mathbf{N}_t \equiv \mathbf{P}_t \mathbf{L}_t \mathbf{P}_t^T \quad (9a)$$

$$\mathbf{N}_t^{-1} \equiv \mathbf{P}_t \mathbf{L}_t^{-1} \mathbf{P}_t^T \quad (9b)$$

in which  $\mathbf{P}_t$  is the truncated set of 1 eigenvectors and  $\mathbf{L}_t$  is the diagonal matrix of corresponding eigenvalues. With these definitions, note that  $\mathbf{N}_t^{-1}$  is not the true matrix inverse of  $\mathbf{N}_t$  but that  $\mathbf{N}_t^{-1} \mathbf{N}_t = \mathbf{P}_t \mathbf{P}_t^T$ . Equations (6) and (8) remain valid nonetheless.

When the problem is formulated this way, it becomes convenient to think of the detection problem in terms of ‘indicators.’ These indicators are obtained by resolving the data set  $\underline{d}$  into  $l$  numbers by projecting the  $l$  retained eigenmodes onto  $\underline{d}$ . Essentially, only  $l$  linear combinations of the original data set are kept. These are the indicators. These indicators can then be used by themselves to solve the multiple climate signal detection problem. The only caveat is that the number of indicators retained must

be greater than or equal to the number of signals to be detected. Otherwise it can be shown that the quantity  $S^T N_i^{-1} S$ , which appears throughout, has no inverse.

### 3. Application to temperature profiles

In this section, the theory of the previous section is applied to calculate the uncertainty  $A$  in the determination of signal amplitudes given a prescription of the natural variability. Equation (8) is used to calculate this uncertainty estimate, which does not involve the use of any data. The result will permit an estimate of how large a signal should be before we can be certain it is not a natural fluctuation of the climate.

The data are monthly average temperature as a function of pressure as measured in one global region for two periods of twelve consecutive months widely spaced in time. The region chosen in this study is the Indian Ocean, which is defined by  $50^\circ$  to  $90^\circ$ E longitude and  $10^\circ$ S to  $10^\circ$ N latitude. The Indian Ocean is chosen because it is anticipated that the natural variability of upper air temperature there is small and a simple radiative-convective model can be used to generate a signal shape. The pressure levels chosen span 10 to 1000 mbars logarithmically:

$$p_i = (10 \text{ mbars}) \times 10^{(i-1)/20} \quad (10)$$

where  $i$  runs from 1 to 41. The elements of the data vector  $d$  are the differences in temperature over a long time baseline for the given pressure levels and the twelve months of the year. The data vector  $d$  consists of temperature changes for 41 different pressure levels and 12 different months of the year, yielding 492 elements for  $d$ , and a 492-by-492 matrix for the natural variability covariance  $N$ .

#### a. The signal pattern

The only pattern sought in this study is the result of increasing concentrations of carbon dioxide. Since only one signal is involved, the signal pattern matrix  $S$  becomes a

vector  $s$  of dimension 492 and the amplitude uncertainty covariance matrix  $\mathbf{A}$  becomes a scalar  $a$ .

The signal pattern is obtained from a one dimensional radiative-convective model (Lindzen et al. 1982) covering 0 to 40-km altitude of a cloudless atmosphere. The cumulus convection scheme is that of Lindzen (1981, 1982) and the radiation scheme is taken from Chou and Suarez (1994). The solar flux is set to  $1374 \text{ W m}^{-2}$ , the surface albedo to 0.15. The diurnal cycle is omitted, but is simulated by setting the solar flux at the surface to half its daylight average. The daylight, average cosine of the zenith angle is set to 0.5. The mixing ratios of methane and nitrous oxide are set to 1.75 ppmv and 0.3 ppmv respectively. Equilibrium temperature profiles are obtained by integrating the model for 600 days with the carbon dioxide mixing ratio set to 330 ppmv and then to 396 ppmv, a 20% increase.

The equilibrium temperature profile as a function of pressure for a carbon dioxide mixing ratio of 330 ppmv is shown in Fig. 1, and the change in the equilibrium temperature profile resulting from increased carbon dioxide is shown in Fig. 2. The latter is the signal pattern  $g$ . It is assumed characteristic of each month of the year.

#### b. *The natural variability*

The natural variability is computed using the 100-year control run of the Geophysical Fluid Dynamics Laboratory (GFDL; Gordon and Stern 1982, Manabe et al. 1991). The model's atmospheric grid is gaussian with 48 longitude elements, 40 latitude elements, and 9 vertical  $\sigma$ -levels spanning the surface to 25 mbars. It is a fully coupled AOGCM. The data, which was obtained from the National Climatic Data Center, are monthly averages over a span of 100 years, giving 1200 time steps of output. The temperature profiles are interpolated onto the pressure levels defined by Eq. (10) logarithmically in pressure.

The natural fluctuations of temperature are obtained by subtracting the average temperature profile and the annual cycle. The natural variability covariance  $\mathbf{N}$  is

calculated by defining the ensemble members over which to average as each year of the 100-year run. This method captures the model's natural variability in upper-air temperature with frequencies less than  $\sim 1 \text{ yr}^{-1}$ , which is appropriate since the simulated data spans just one year in time.

*c. Signal adjoints and uncertainties*

The optimal fingerprints (signal adjoints) and the uncertainty in signal amplitude are calculated. The signal adjoints are found using Eq. (6) and the amplitude uncertainties are calculated using Eq. (8). The climate variability is a truncated version of the full covariance, as defined by Eq. (9). The profile of the range of temperature fluctuations for August, is shown in Fig. 3.

1) NO INTERMONTH CORRELATION

At first, the fluctuations of the climate are considered independent from month to month but not from vertical level to level. Detecting the signal  $\mathbf{s}$  turns into twelve independent problems, one for each month of the year, each with its own signal adjoint vector  $\mathbf{c}_i$ , amplitude estimate  $\alpha_i$ , and amplitude covariance  $a_i$ . The index  $i$  is for the month of the year, and equations (6) and (8) apply to each month individually. The natural variability covariance  $\mathbf{N}_i$  is computed for each month, and the eigenmodes and eigenvalues are found for each  $\mathbf{N}_i$ . For example, the first four eigenmodes for August are shown in Fig. 4.

Recall that the matrix  $\mathbf{P}_l$  is defined as a subset of the complete eigenvector set for the climate variability covariance matrix  $\mathbf{N}$ . Here, the eigenvector matrix is composed of the  $l$  modes with the largest eigenvalues. The degree to which each of these modes contributes to detecting the signal  $\mathbf{z}$  depends on how much of the signal is described by the eigenmode and how much of the climate's natural variability is in that mode. To evaluate the former dependence, the degree to which the signal  $\mathbf{z}$  projects onto each

mode is given by

$$\underline{\phi} = \mathbf{P}_t^T \underline{z} \quad (11)$$

The latter dependence is just the eigenvalue of that mode. The uncertainty covariance  $a$ , otherwise given by Eq. (8), can be rewritten as

$$a = \left( \sum_{k=1}^l \frac{\phi_k^2}{2\lambda_k} \right) \quad (12)$$

in which  $\phi_k$  is the  $k$ 'th element of  $\underline{\phi}$ ,  $\lambda_k$  is the  $k$ 'th eigenvalue, and the extra factor of 2 is included because a difference must be taken between two different years. If  $\alpha_m$  is the amplitude of the signal as it might emerge in the data, then the signal-to-noise ratio SNR of the detection is given by  $\alpha_m/a^{1/2}$ , or

$$\text{SNR}^2 = \alpha_m^2 \sum_{k=1}^l \frac{\phi_k^2}{2\lambda_k} \quad (13)$$

Figure 5 shows twelve spectra of  $\phi_k^2$  and  $2\lambda_k$ , one for each month of the year. The ratio of  $\phi_k^2$  to  $2\lambda_k$  for each eigenmode is the amount of  $\text{SNR}^2$  contributed by each indicator given  $\alpha_m = 1$ , or the presence of the signal  $\underline{z}$  in the data  $\underline{d}$ . There is a clear cascade of eigenvalues for each month, but the projections  $\phi_k^2$  do not cascade as smoothly. In fact, beyond some eigenmode number, the projections  $\phi_k^2$  become highly irregular, reflecting the fact that the signal  $\underline{z}$  will project onto an eigenvector regardless of its eigenvalue. Depending on what set of modes is retained as the indicators, it seems possible to obtain any signal-to-noise ratio for detecting the climate signal  $\underline{z}$  we desire. This deserves closer inspection.

In general, the modes of variability with the largest eigenvalues are associated with the largest vertical features, and the modes with the smallest eigenvalues with the finest vertical features. Thus, the coarsest features of the signal  $\underline{z}$  are represented by the modes with the largest associated variability. To illustrate this point, the signal is projected onto the first  $l$  modes of variability and expanded by those same modes:

$$\underline{z}_R = \mathbf{P}_t \mathbf{P}_t^T \underline{z} \quad (14)$$

where  $s_R$  is the reconstructed signal and  $P$  is the matrix containing the first  $l$  modes of variability. The reconstructed signal  $s_R$  is dependent on the number of modes included ( $l$ ), and is shown in Fig. 6 for  $l$  from 1 to 6 using the eigenvectors for August. The first five modes describe the coarsest scales of the signal well enough, such that the remaining differences between the signal and its reconstruction are more likely the result of a flawed model than details of a realistic signal. There is no reason to trust a 1-d radiative-convective model (or any other model) to give a realistic signal shape down to such fine detail. Thus, the higher order modes cannot be justifiably used as indicators in this detection problem and only the first five modes are used ( $l = 5$  in Eq. (9)).

Table 1 gives the signal-to-noise ratio for each month given  $l = 5$ . Recall that  $\alpha_m = 1$  reflects the consequences of a 20% increase in carbon dioxide. For purposes of comparison, table 1 also gives the SNR that is obtained if only the surface temperature ( $p = 1000$  mbars) is used. The signal is most probably detected in August, with an SNR of 1.80 ( $\alpha_m = 1$ ). Assuming a carbon dioxide growth rate of 0.5% per year, it would take 22 years ( $(40 \text{ years})/1.80$ ) to obtain a 1-sigma detection of anthropogenically-induced warming in August upper air temperatures. In comparison, it would take 43 years ( $(40 \text{ years})/0.93$ ) to obtain a 1-sigma detection using the August surface temperature alone.

Many previous detection studies have used only surface temperatures to detect climate signals, so it is instructive to estimate how many extra independent indicators one gains by using upper-air temperatures in addition. The ratio of the SNR obtained using upper-air temperatures to the SNR obtained using surface temperature is approximately the square-root of the number of independent indicators compared to just one indicator for the surface temperature. By this method, the number of independent indicators is approximately 2 to 3 times the number of surface temperature indicators, according to table 1.

## 2) WITH INTERMONTH CORRELATION

Next, the fluctuations are assured correlated between levels and months of the year. The signal  $\underline{s}$  contains 492 elements and bears the same structure for each month of the year, as shown in Fig. 2. Equations (6) and (8) applied in full.

Figure 7 shows the spectra of both the projection of the signal onto each mode of variability and twice the variance  $\lambda_k$  of that mode. Recall that all months of the year are coupled together and thus only a single spectrum is necessary. As before, it is possible to obtain a nearly infinite SNR in detection if every mode is included. In this case, the signal is spread over many more modes than previously, because in coupling the months of the year together more modes of variability are introduced. As a consequence, how to truncate the series of projections becomes a more difficult decision. Figure 8 shows the sum of the first  $l$  square-projections  $\phi_k^2$  normalized by the square of the signal  $s^2$ :

$$\text{Cum } \phi^2(l) = \left( \sum_{k=1}^l \phi_k^2 \right) / \left( 12 \sum_{i=9}^{41} s_i^2 \right). \quad (15)$$

Recall that  $\phi_k$  is the  $k$ 'th element of  $\phi$  as defined by Eq. (11). The first eight elements of  $\underline{s}$  are dropped because the variability, which is computed using the GFDL AOGCM, **dots** not span pressures between 10 and 25 mbars. The cumulative square projection can be thought of as the fraction of the signal accounted for after including the  $l$  modes with the largest variances.

The climate variability  $\mathbf{N}_l$  is defined by truncating the set of eigenmodes according to Eq. (9). After truncation, the remaining  $l$  modes are those with the  $l$  largest eigenvalues. The number of modes retained is enough to give a cumulative  $\phi^2$  of 0.90, about the same cumulative  $\phi^2$  obtained by including 5 modes in the previous section. This mandates keeping about 60 modes. The adjoint vector, which spans all months of the year, is shown in Fig. 9. The SNR for this method is 5.04. If, however, the first 72 modes are used, then the SNR for detection becomes 6.06. Table 2 contains a list of the

SNR for certain numbers of modes included (1). Clearly, the detectability of a signal is heavily dependent on the  $l$  indicators used in the detection.

In comparison, the SNR for detecting a signal induced by a 20% increase in carbon dioxide ( $\alpha_m = 1$ ), using only the surface temperature with intermonth coupling, is 3.05. This is found by first taking the subset of the total climate covariance  $\mathbf{N}$  corresponding to the 1000-mbar temperature fluctuations, defining it as  $\mathbf{N}_s$ , a 12-1~y-12-element matrix. Then the signal is defined as  $\xi_s$ , a 12-element vector, each element of which is set to the element of the signal  $\xi$  corresponding to 1000 mbars. The surface SNR becomes

$$\text{SNR}_s^2 = \alpha_m^2 \left( \xi_s^T \mathbf{N}_s^{-1} \xi_s \right). \quad (16)$$

Thus, with intermonth coupling, it would take 7 years ((40 years)/5.04) to obtain a 1-sigma ( $\alpha_m = 1/5.04$ ) detection of carbon dioxide-induced warming using upper air temperature but 13 years ((40 years)/3.05) using only surface air temperature.

Certainly, natural fluctuations of the climate can generate temperature trends over a 7-year timescale that can swamp the effects of warming by increased greenhouse gases. Provided that the model used to simulate the variability approximates decadal timescale variability well, the statistics done here properly take such natural trends into account. Note that a 1-sigma detection means that there is a 32% chance that a natural fluctuation of the climate will overwhelm the signal. This is not an insignificant probability, and thus at least a 3-sigma detection should be sought.

The results for SNR obtained so far can be easily modified by selecting a different set of modes to redefine the climate variability. Another plausible approach is to select only those modes which account for most of the signal. This amounts to sorting by descending squared-projections  $\phi_k^2$  as defined by Eq. (11). The cumulative square projection  $\text{Cum } \lambda^2(1)$  (c.f. Eq. (15)) is then defined after resorting, and the signal-to-noise ratio can be redefined accordingly (cf. Eq. (13)). The eigenvalues of the variability  $\lambda_k$  are resorted by decreasing  $\phi_k^2$  as well.

The  $\text{SNR}/\alpha_m$  is plotted as a function of the cumulative square projection in Fig. 10. Logically, as more modes are included, the SNR increases. In fact, it does so steadily until about 80% of the signal is accounted for, at which point an abrupt jump in the SNR occurs. The jump occurs because of the contribution of mode 69 in Fig. 7. By itself, this mode can generate an SNR of 2.53 even though it only contributes to 0.0064 of the square of the signal shape  $|g|^2$ .

There are many modes which can contribute immensely to the signal-to-noise ratio of the detection of the carbon dioxide warming signal, but all of these correspond to very small components of the input signal. If in fact we could impute confidence in their being important components of the signal, then these are the components which should be most sought after in signal detection studies and observations. If on the other hand there is no reason to believe that these components are trustworthy indicators of the presence of the signal, then it would be a mistake to use them at all. In this case, there is no reason to believe that the component of the signal which projects onto mode 69 of the variability is a realistic component of the signal. There is no reason to assume the radiative-convective model is correct enough to give us certainty in this mode.

In the end, the best estimate of the SNR obtainable is that obtained before mode 69 is included. The SNR obtained by including the first  $l$  modes with the largest projections onto the signal is 4.11 for  $\alpha_m = 1$ . This implies that a 1-sigma detection of carbon dioxide-induced warming should take about 10 years when one year's worth of monthly averages is compared to another year's worth of monthly averages over the Indian Ocean.

#### 4. Discussion

The evidence for greenhouse gas-induced warming will be convincing when the significance of detection exceeds about 3-sigma. Given a 1-sigma detection time of about 10 years, the 3-sigma time is about 30 years, or about three fourths of the signal shown in Fig. 2. Given this figure, several complicating aspects of detecting this signal remain.

First, optimal detection requires a certain degree of accuracy in the observations to be used. Secondly, the signal being sought must be computed with some quantifiable confidence. Third, the background variability of the atmosphere required by optimal detection can only be provided by imperfect models. Finally, the work presented in this paper needs to be expanded to encompass horizontally global coverage and different realistic data types.

The philosophy behind optimal detection is to identify a forced signal in climate data even when it is very weak. For optimal detection to apply to real data, the observations must certainly be able to recognize such a signal in the absence of climate noise. Hence, the observations must have systematic errors less than the temperature differences involved, which are about 0.5 K. While this seems like an extraordinary restriction, there are potential methods of observing the Earth's climate with such small systematic errors. Such methods include GPS radio occultations and high spectral resolution infrared spectroscopy. Then again, even if the systematic errors are comparable to 0.5 K, they are troublesome only if they can possibly imitate the form of the temperature signal. For instance, a systematic error which is uniform across all vertical levels can be distinguished from the expected signal pattern which is not uniform across vertical levels. If estimable, the systematic errors can be properly accounted for by adding their covariance to the natural variability covariance matrix and proceeding as discussed in this paper.

Optimal fingerprinting and hence attribution of greenhouse gas-induced global warming requires prior knowledge of the form of the forced climate signal, which can only be estimated using imperfect models. While some bulk properties of the signal may be predicted reliably, the sensitivity of optimal fingerprinting to small components of the uncertain signal shape is troublesome. The methods used in this work to cut out those components which give unrealistic signal-to-noise ratios are *ad hoc*, there being no alternative technique to formally consider uncertainties in signal shapes. Since the

difficulty is a direct consequence of uncertainties in input quantities, it seems that a Bayesian analysis would be the best way to approach this problem formally.

In optimizing the detection and attribution of greenhouse gas-induced global warming, a prescription of the natural variability of the atmosphere is necessary so that specific components of the forced signal can be emphasized over others in organizing the data. The prescription of the variability must come from AOGCM's and is thus flawed. Ultimately, confidence in the prescriptions can be gained when the processes of the models are checked statistically against data and subsequently improved. Methods for such testing are described elsewhere (J Iaskins et al. 1997, Polyak 1996). No practical method for improving models once this testing has taken place has been formally presented. In the meantime, one must try to avoid components of simulated variability which are exceedingly small and use as many different prescriptions of the variability as possible.

Even though the base timescale estimated for detecting (and attributing) carbon dioxide warming of the atmosphere is approximately 10 years for a 1-sigma detection, much more can be done to possibly improve upon this figure. This study only concerned monthly average temperatures in the region of the Indian Ocean. Subsequent work will expand to horizontally global coverage, first by including more regions in addition to the Indian Ocean. Most likely there are several regions of the globe whose variabilities are largely uncorrelated, the result of which will be to augment the potential SNR of a detection by the square-root of the number of independent regions. Secondly, in subsequent studies, different types of data, such as those mentioned above, will be examined as potential data types to reveal greenhouse gas-induced global warming. Actual data types must be simulated because temperature profiles in the atmosphere are never truly measured: it is only sonic kernel of temperature profiles (and water vapor and cloud profiles) which is measured. Thirdly, subsequent work will include the forms of other potential signals in order to eliminate the possibility of filter leakage (Leroy

**1998).** For example, a signal in temperature profiles can be produced by an independent warming of the ocean surface layer which probably has similarities to greenhouse gas-induced warming. Confusion between the two signals can be eliminated by simply including both in the set of signals  $S$  described in section 2.

*Acknowledgements.*

This research was supported by Code YSC of the National Aeronautics and Space Administration. I thank Gerald North (Texas A&M) and especially Richard Goody (JPL) for helpful discussions. Also, I thank Tom Ross (NCDC) for supplying me with the upper-air output of the GFDL model control runs and Arthur Hou (GSFC) for his 1-d radiative-convective model. This work was supported by a grant from NASA Code YSC.

## REFERENCES

- Angell, J. K., 1988: Variations and trends in tropospheric and stratospheric global temperatures, 1958-87. *J. Climate*, **1**, 1296-1313.
- Aumann, G.H., and R. Pagano, 1994: The atmospheric infrared sounder on EOS. *Opt. Eng.*, **32**, 776-784.
- Bell, T.L., 1986: Theory of optimal weighting of data to detect climatic change. *J. Atmos. Sci.*, **43**, 1694-1710.
- Chou, M.-I.), and M.J. Suarez, 1994: An efficient thermal infrared radiation parameterization for use in general circulation models. NASA Technical Memorandum 104606, Vol. 3, 85 pp.
- Gaffen, D. J., 1994: Temporal inhomogeneities in radiosonde temperature records. *J. Geophys. Res.*, **99**, 3667-3676.
- Goody, R., J. Anderson, and G. North, 1997: The value for climate predictions. Submitted to *Bull. Am. Met. Soc.*
- Gordon, C.T., and W.F. Stern, 1982: A description of the GFDL global spectral model. *Mon. Wea. Rev.*, **110**, 625-644.
- Haskins, R.D., R.M. Goody, and L. Chen, 1997: A statistical method for testing a general circulation model with spectrally resolved satellite data. *J. Geophys. Res.*, **102**, 16563-16581.
- Hasselmann, K., 1997: Multi-pattern fingerprint method for detection and attribution of climate change. *Climate Dyn.*, **13**, 601-611.
- , 1993: Optimal fingerprints for the detection of time-dependent climate change. *J. Climate*, **6**, 1957-1971.
- Hegerl, G.C., K. Hasselmann, U. Cubasch, J.F.B. Mitchell, E. Roeckner, R. Voss, and J. Waszkewitz, 1997: Multi-fingerprint detection and attribution analysis of greenhouse gas, greenhouse gas-plus-aerosol and solar forced climate change. *Climate Dyn.*, **13**, 613-634.

- Hegerl, G.C., K. Hasselmann, U. Cubasch, J.F.B. Mitchell, F. Roeckner, R. Voss, and J. Waszkewitz, 1996: On multi-fingerprint detection and attribution of greenhouse gas- and aerosol-forced climate change. Report no. 207, Max-Planck-Institut für Meteorologic, Hamburg.
- , H. von Storch, K. Hasselmann, B.D. Santer, U. Cubasch, and P.D. Jones, 1996: Detecting greenhouse-gas-induced climate change. with an optimal fingerprint method. *J. Climate*, 9, 2281-2306.
- Houghton, J.T., and L. G. Meira Filho, 1996: *Climate Change 1995. The IPCC Second Scientific Assessment*. Cambridge University Press, 572 pp.
- Kursinski, E.R., and Coauthors, 1996: Initial results of radio occultation observations of Earth's atmosphere using the global positioning system (GPS). *Science*, 271, 1107-1109.
- Kursinski, E.R., G.A. Hajj, J.T. Schofield, R.P. Linfield, and K.R. Hardy, 1997: Observing Earth's atmosphere with radio occultation measurements using the Global Positioning System. *J. Geophys. Res.*, 102, 23429-23465.
- Leroy, S. S., 1997: Measurement of geopotential heights by GPS radio occultation. *J. Geophys. Res.*, 102, 6971-6986.
- Leroy, S. S., 1993: Detecting climate signals: some Bayesian aspects. *J. Climate*, in press.
- Lindzen, R. S., A. Y. Hou, and B.F. Farrell, 1982: The role of convective model choice in calculating the climate impact of doubling CO<sub>2</sub>. *J. Atmos. Sci.*, **39**, 1189-1205.
- , 1981: Some remarks on cumulus parameterization. *Clouds in Climate: Modeling and Satellite Observational Studies*, Rep. of Workshop held at NASA Goddard Institute for Space Studies, 222 pp.
- Manabe, S., R.J. Stouffer, M.J. Spelman, and K. Bryan, 1991: Transient responses of a coupled ocean-atmosphere model to gradual changes of atmospheric CO<sub>2</sub>. Part I: annual mean response. *J. Climate*, 4, 785-818.

- North, G.R., 1996: *GPS-CLIM: A Microsatellite Constellation to Test Climate Models*.  
Proposal to NASA's Earth System Science Pathfinder Program, Jet Propulsion  
Laboratory, California Institute of Technology.
- North, G.R., K.-Y. Kim, S.S.P. Shen, and J.W. Hardin, 1995: Detection of forced  
climate signals. Part I: filter theory. *J. Climate*, 8, 401-408.
- Polyak, I., 1996: Observed versus simulated second-moment climate statistics in GCM  
verification problems. *J. Atmos. Sci.*, **53**, 677-694.
- Santer, B.D., K.E. Taylor, J.E. Penner, T.M.L. Wigley, U. Cubasch, and P.D. Jones,  
1995: Towards the detection and attribution of an anthropogenic effect on climate.  
*Climate Dyn.*, **12**, 771-780.
- Santer, B.D., and Coauthors, 1996: A search for human influences on the thermal  
structure in the atmosphere. *Nature*, **382**, 39-46.

## Table Captions

TABLE 1. The signal-to-noise ratio for detecting the signal from a 20% increase in carbon dioxide in temperature profiles and surface temperatures averaged over the Indian Ocean. Like months are differenced (e.g. January to January, etc.). The signal is calculated using a radiative-convective model and the variability is taken from the GFDL 100-year control run but assumed uncorrelated between months.

Month	SNR/ $\alpha_m$	Surface SNR/ $\alpha_m$
January	1.457	1.187
February	1.307	1.186
March	1.471	0.952
April	1.489	1.120
May	1.752	1.100
June	1.754	1.034
July	1.475	0.860
August	1.802	0.926
September	1.627	1.010
October	1.670	1.019
November	1.643	1.051
December	1.641	1.163

TABLE 2. The signal-to-noise ratio for detecting the signal from a 20% increase in carbon dioxide in temperature profiles after including the first  $l$  modes of variability. Also included is the fraction of the signal accounted for after including the first 1 modes of variability.

$l$	Cum $\phi^2(l)$	SNR/ $\alpha_m$
12	0.625	2.337
24	0.754	3.025
36	0.813	3.627
48	0.868	4.719
60	0.877	5.042
72	0.891	6.059
84	0.904	8.071
96	0.908	11.843

## Figure Captions

FIG. 1. The equilibrium temperature profile of a 1-d radiative-convective model with CO<sub>2</sub> concentration of 330 ppmv.

FIG. 2. The difference between a radiative-convective equilibrium temperature profile given CO<sub>2</sub> concentration of 396 ppmv and one given a CO<sub>2</sub> concentration of 330 ppmv.

FIG. 3. The variance range of the monthly average temperature as a function of pressure for August over the Indian Ocean as determined by the first 100 years of the GFDL 1000-year control run.

FIG. 4. The first four eigenvectors of variability for monthly average August temperature over the Indian Ocean. The eigenvectors are scaled by the square-root of their eigenvalues. The variability was calculated using the first 100 years of the GFDL 1000-year Control run. The first eigenmode contains 41% of the total variance (A), the second contains 31 % (B), the third contains 15% (C), and the fourth contains 5% (D).

FIG. 5. Spectra for the squared-projections and variability eigenvalues for each month over the Indian Ocean. The signal is determined using a 1-d radiative-convective model and the climate “noise” is taken from the first 100 years of the GFDL 1000-year control run. The units are K<sup>2</sup>, the open diamonds are for twice the eigenvalues, and the solid diamonds are for the squared-projections.

FIG. 6. Reconstructions of the +20% CO<sub>2</sub> signal given the eigenvectors for August. Reconstructions are shown after the first  $l$  eigenvectors are included for  $l = 1, \dots, 6$  corresponding to A-F. The heavy line is the reconstruction and the lighter line is the synthesized signal.

FIG. 7. Spectrum for the squared-projections and variability eigenvalues when the months of the year are coupled. The open squares represent the squared-projections  $\phi_k^2$  and the smooth line represents twice the eigenvalues.

FIG. 8. The sum of the squared-projections of the CO<sub>2</sub>-increase signal onto the first 1 modes. The sum is normalized by the square of the signal  $|\xi|^2$  over the pressure range spanned by the GFDL model. The eigenmodes are sorted by decreasing eigenvalue.

FIG. 9. The optimal adjoint using the first 60 eigenvectors of variability. The units of the abscissa are  $1 \text{ O}^\circ \text{ } ^\circ\text{K}^{-1}$ , and multiplication of this vector onto the difference between monthly average temperatures separated by many years gives the amplitude of the signal in units of a 20% increase in carbon dioxide.

FIG. 10. The amount of signal-to-noise available by including the first  $l$  indicators versus the normalized cumulative squared-projection. The indicators are sorted by decreasing squared-projection  $\phi_k^2$  onto the eigenvectors of the climate variability.

Figure 1

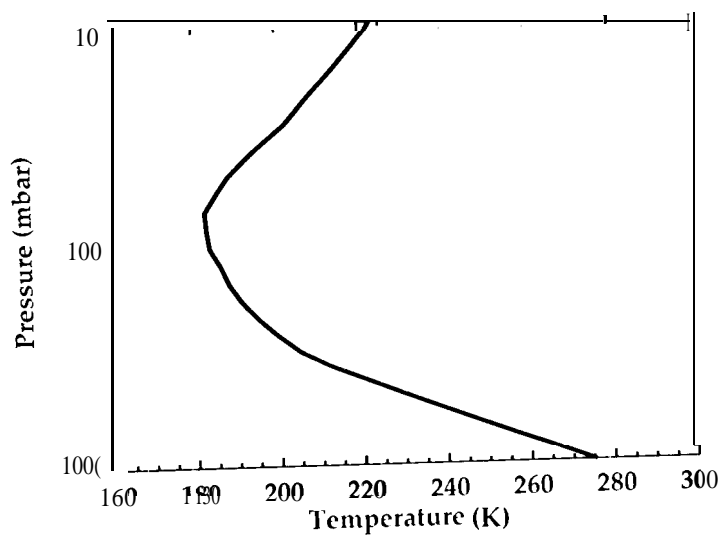
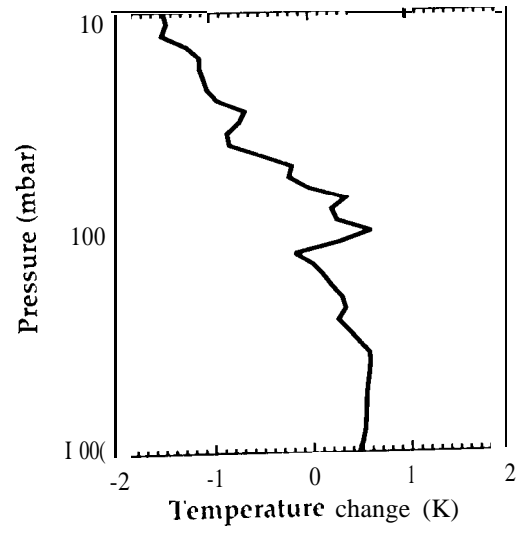
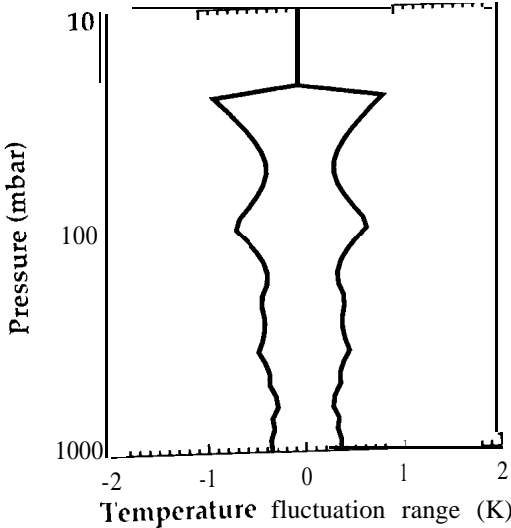


Figure 2



**Figure 3**



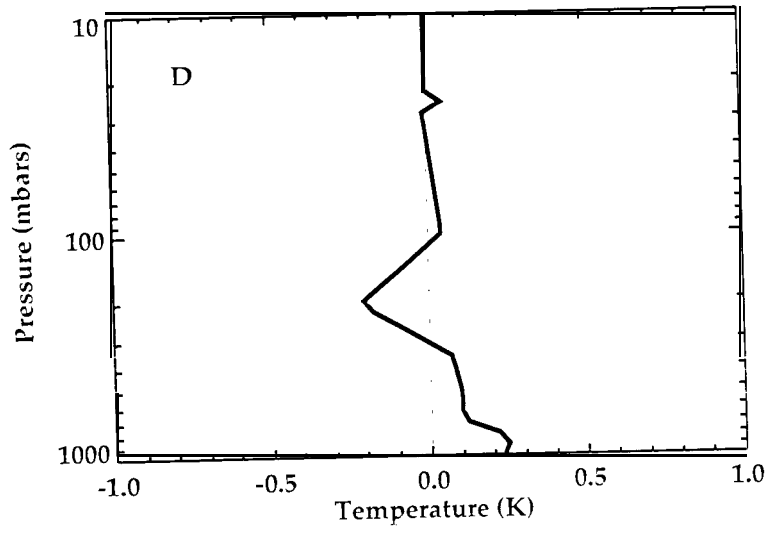
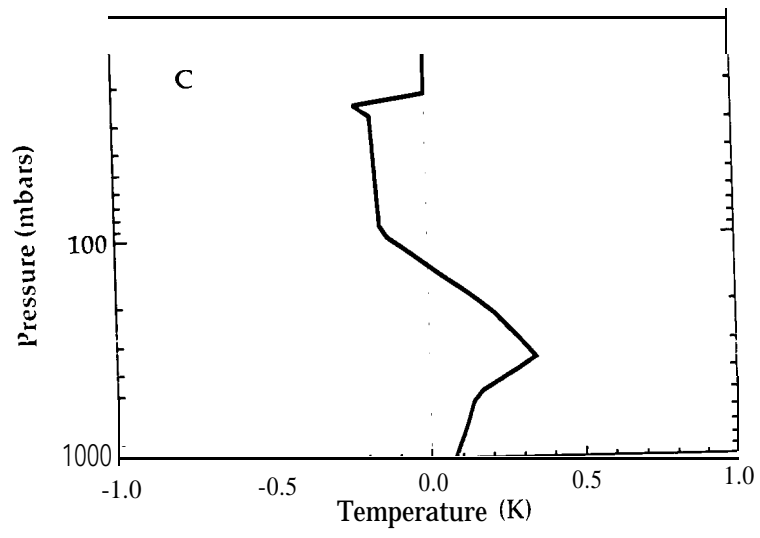
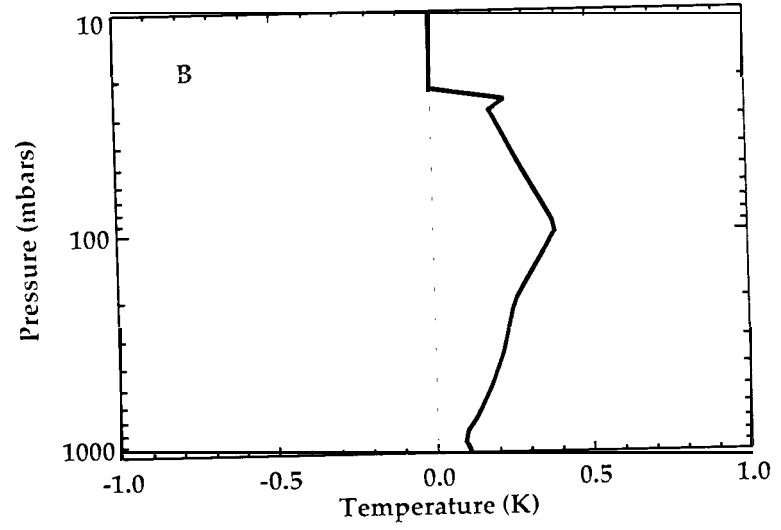
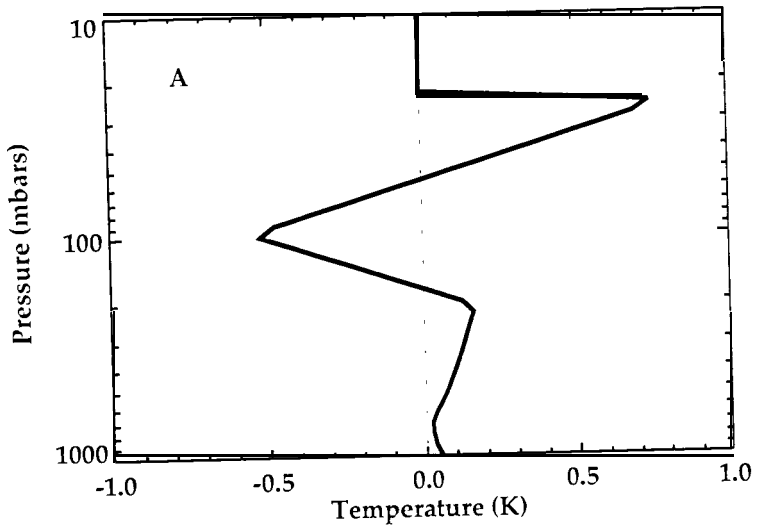


Figure 4

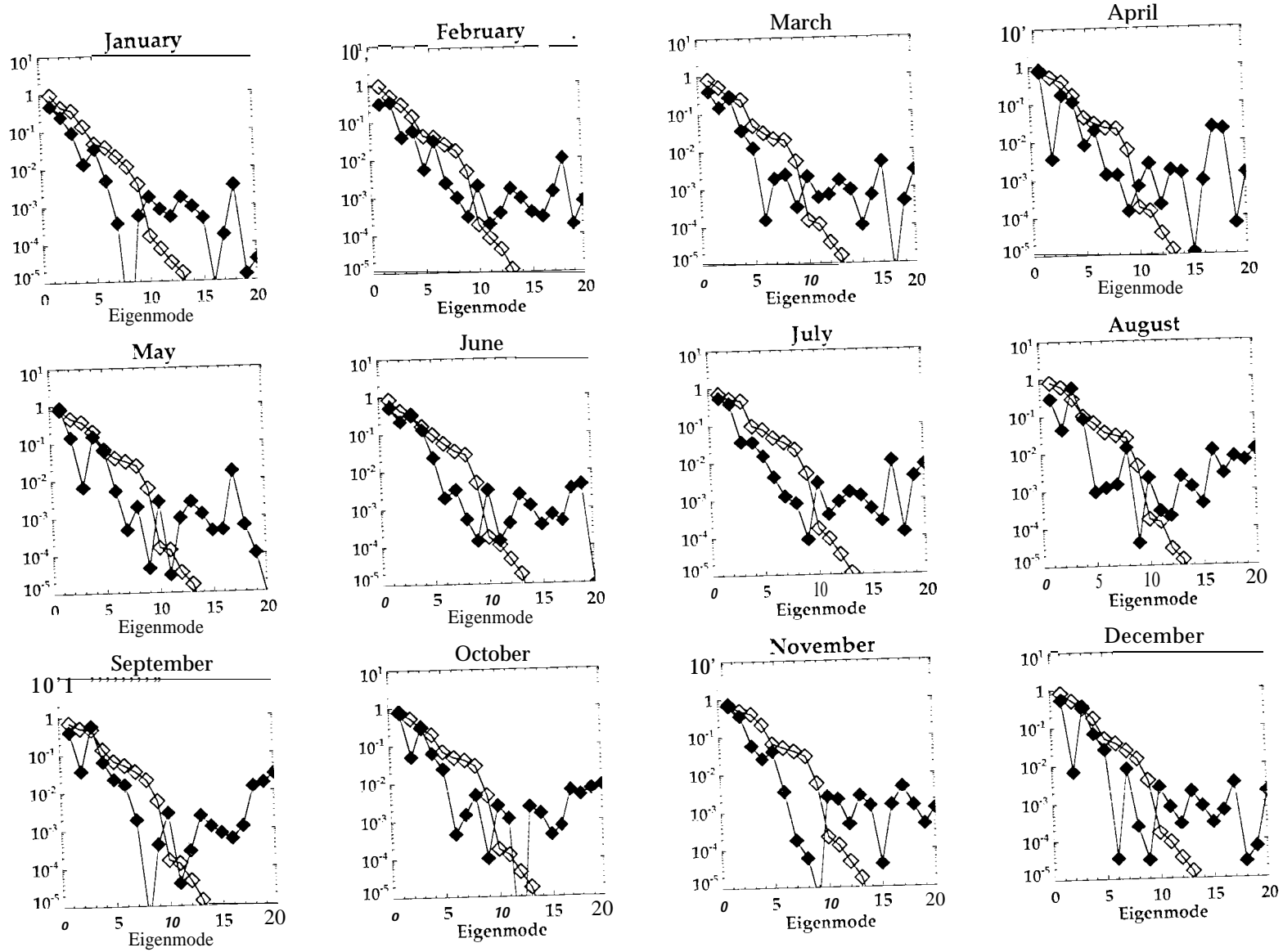
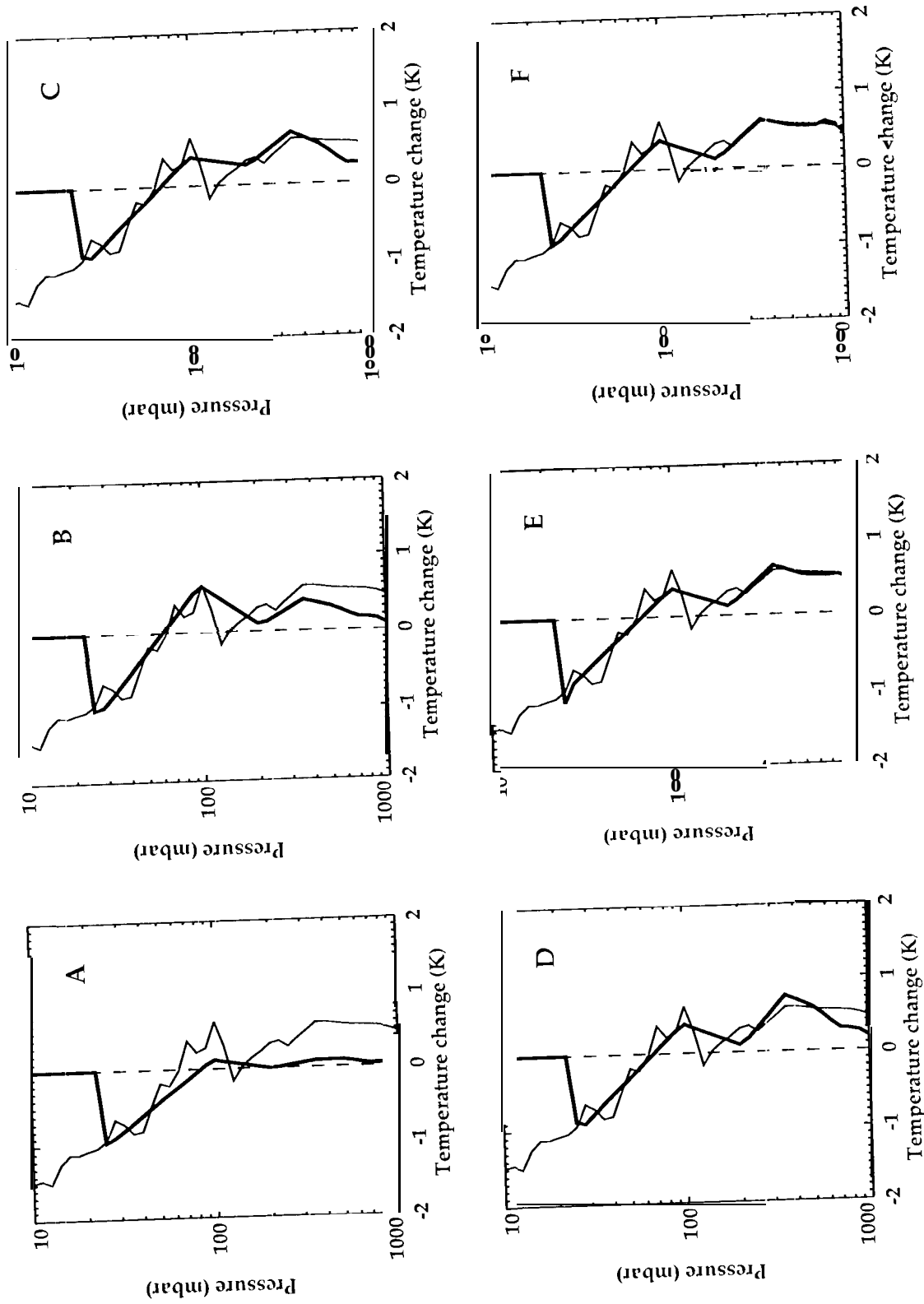
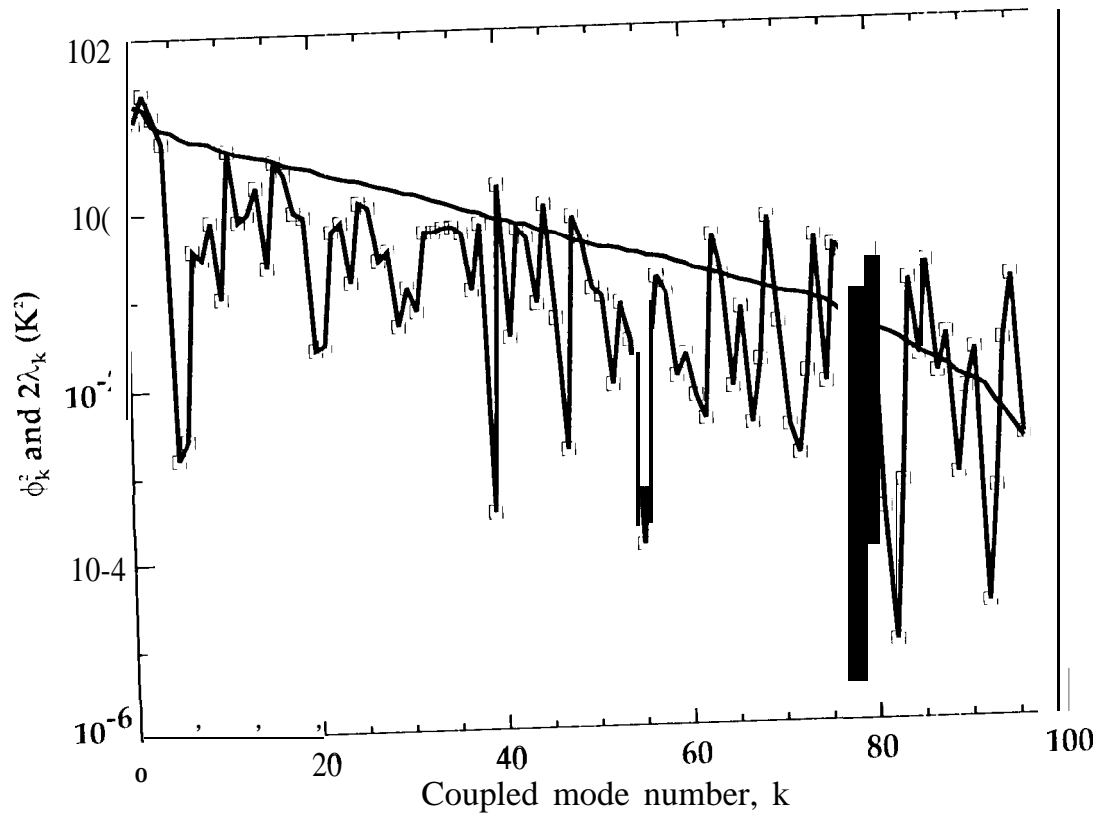


Figure 5

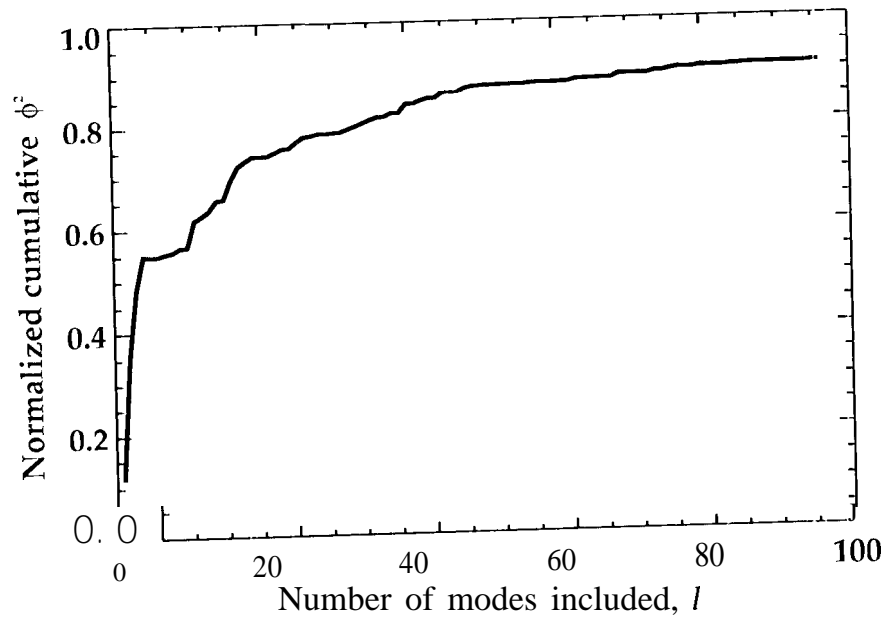
Figure 6



**Figure 7**



**Figure 8**



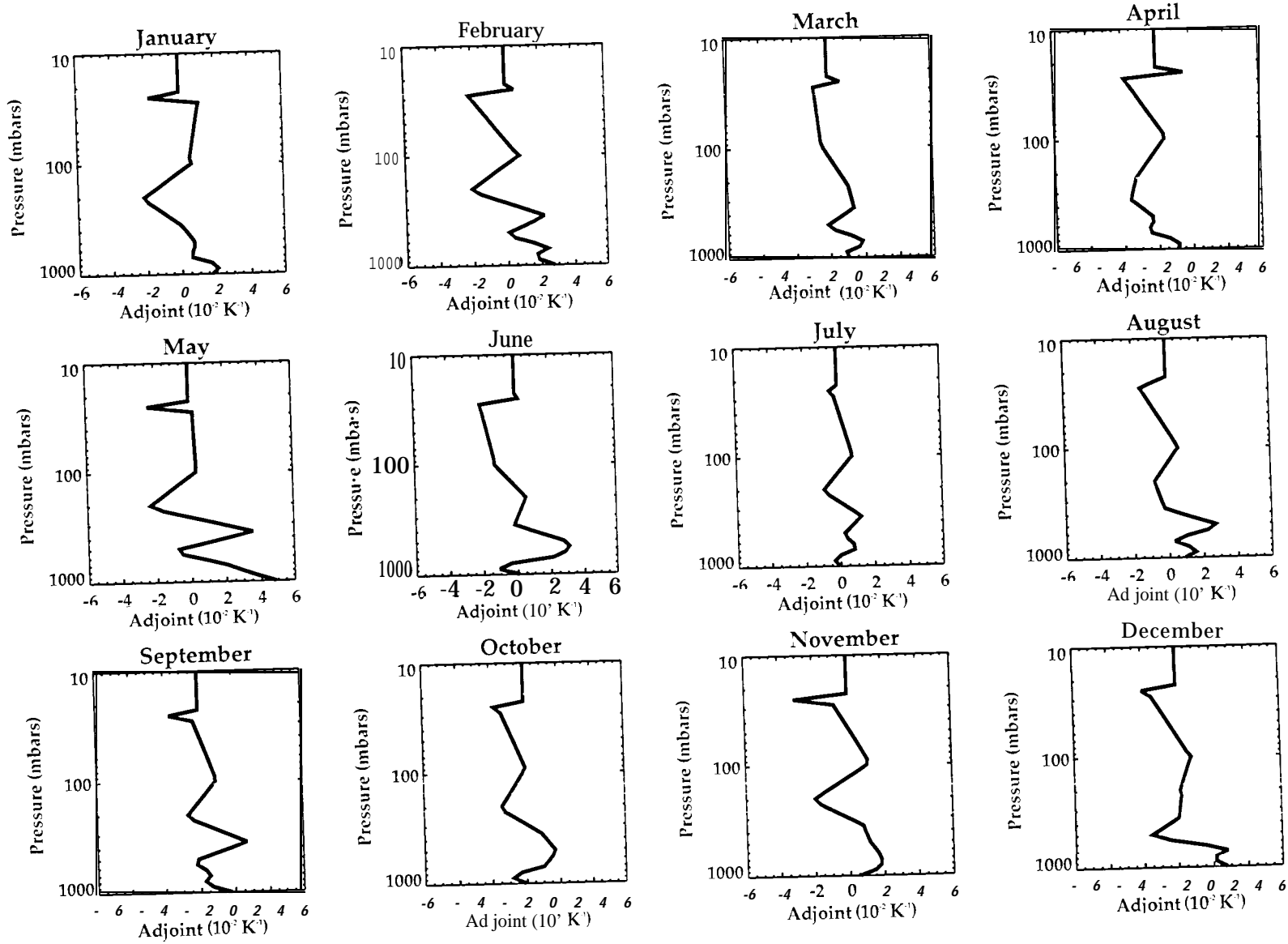


Figure 9

Figure 10

